



### **Science Arts & Métiers (SAM)**

is an open access repository that collects the work of Arts et Métiers Institute of Technology researchers and makes it freely available over the web where possible.

This is an author-deposited version published in: <https://sam.ensam.eu>  
Handle ID: <http://hdl.handle.net/10985/23355>

#### **To cite this version :**

Gwenaëlle CHEBIL, Pierre LAPOUGE, Yves RENOLLET, Cécile DAVOINE, Marc THOMAS, Matthieu SCHNEIDER, Véronique FAVIER - Study of spatter ejections during laser-powder bed fusion process for aluminum alloys - Journal of Laser Applications - Vol. 33, n°4, p.042047 - 2021

Any correspondence concerning this service should be sent to the repository

Administrator : [scienceouverte@ensam.eu](mailto:scienceouverte@ensam.eu)



# STUDY OF SPATTER EJECTIONS DURING L-PBF PROCESS FOR ALUMINUM ALLOYS

Gwenaëlle Chebil<sup>1</sup>, Pierre Lapouge<sup>2</sup>, Yves Renollet<sup>1</sup>, Cécile Davoine<sup>1</sup>, Marc Thomas<sup>1</sup>, Véronique Favier<sup>2</sup>,  
Matthieu Schneider<sup>2</sup>

<sup>1</sup>DMAS, ONERA – The French Aerospace Lab, Paris Saclay University, 92320 Châtillon, France  
<sup>2</sup>PIMM, Arts Et Métiers Institute of Technology, CNRS, Cnam, HESAM University, 75013 Paris, France

## Abstract

During L-PBF process on aluminum alloys, instabilities such as spatter ejections result from the laser-matter interaction. These spatters create a variety of defects and affect the mechanical properties of the final parts. To help understanding this phenomenon, a global method was developed, combining experimental study and image analysis. This system provides statistic information on spatter population (radius, velocity, direction and emission rate) and the idea of pollutant spatter is defined. Four aluminum alloys are compared. The results show the oxygen content in the fabrication chamber has no effect on the spatter ejection dynamic. The spatter velocity, angle of ejection and size increase with the intensity. Also, significant differences are noticed between the different alloys.

## Introduction

Laser-Powder Bed Fusion (L-PBF) is the most widespread additive manufacturing (AM) process for metal. It can create a solid part layer by layer, by scanning powder material with a laser beam. Additive manufacturing of aluminum alloys presents major interests for cutting-edge sectors (aeronautics and transport), both for weight saving and property enhancement. This leads manufacturers to design new grades specifically for AM. However, some difficulties subsist when processing metals with L-PBF, and especially regarding aluminum grades. The fast solidification and cooling rates resulting from the laser-powder bed interaction induce complex hydrodynamic behaviors and instabilities. As a result of such instabilities, a significant amount of spatters is ejected from the powder bed and the molten pool, thereby creating a variety of defects that might affect roughness and mechanical properties. Moreover, these spatters deteriorate the reusability of the powder.

Different types of spatters have been identified in the literature. Ly *et al.* distinguished the metal vapor-driven particles entrainment from the liquid droplets ejection induced by recoil pressure [1]. The first ones have a size close to the feedstock powder, and therefore are less

problematic than the second ones, which can reach up to 100  $\mu\text{m}$  radius according to Gunenthiram *et al.* [2]. Wang *et al.* discussed the difference between the spatters as coming from the melt-pool [3]. As for Liu *et al.*, they pointed out that spatters ejected during L-PBF could have different impacts on the final parts regarding their size [4]. While the smallest ones are recoated with powder and remelted at the following layer, the biggest ones on the contrary hinder the recoating process and could only be partially remelted. As a consequence, by polluting the powder bed, the spatters create irregularities during L-PBF process. They are also responsible for a diminution of the final parts density and a deterioration of the surface roughness. In the specific case of aluminum alloys, Lutter-Günther *et al.* described that spatters show an increased oxygen content compared to the feedstock powder as they carry away part of the oxide layer at the melt-pool's surface [5]. They noted that the oxygen content in the final part is lower than in the feedstock powder. Thereby, spatters are locally responsible for material's chemical modification. A high content of alumina in the final piece tends to lower the mechanical properties by initiating stress during dynamic loading.

Spatter ejections have long been observed during laser welding, by You *et al.* among others [6]. They correlated the total volume of ejected spatters to the weld quality. It becomes more complicated to observe spatter ejections during L-PBF because the ejected particles are not only liquid droplets ejected from the melt-pool but also powder particles ejected from the powder bed. The size distribution of the ejected particles spreads, with the addition of smaller powder particles as well as bigger powder aggregates. The total number of ejected particles reflects the level of interaction between the melt pool and the vapor plume. Moreover, due to the small build chamber, AM machines are not easily equipped with visualization instruments. For instance, Liu *et al.*, Wang *et al.*, Repossini *et al.*, Barrett *et al.* or else Taheri *et al.* positioned cameras outside of commercial AM machines to observe the spatter ejections mechanisms [3], [4], [7]–[9]. These visualizations allow real time monitoring of the process

stability. On the other hand, Ly *et al.*, Traore *et al.*, Guo *et al.* and Young *et al.* designed specific observation setups [1], [10]–[12]. With X-Ray, Guo *et al.* and Young *et al.* managed to look directly at the melt-pool for analysis of the spatter formation mechanisms [11], [12]. All of these studies are based upon a global observation of spatters, with a qualitative approach distinguishing the spatters according to their size or their ejection mechanism.

The current work describes a new analysis method for spatter ejections during L-PBF process. It draws the spatters trajectories and provides statistic distribution of spatter population regarding their radius, velocity, direction and emission rate.

## Experimental procedure

### Open L-PBF setup

Figure 1 presents the open L-PBF cell designed for this experimental study. An Yb:YAG laser source is focused into a 150  $\mu\text{m}$  diameter spot with a “top hat” distribution. A camera is lined up with the laser source and fixed. The frame rate is 10 kfps and a field of 4 mm x 11 mm is captured. The powder sample is placed into a small fabrication chamber at ambient pressure, with controlled working atmosphere. Argon is injected through a diffuser inlet, creating an inert atmosphere in the chamber and maintaining constant pressure. Oxygen content is measured with an  $\text{O}_2$  analyzer. Three windows on the chamber allow laser access and viewing of the interaction. A filter is used to prevent undesired laser reflections. A motorized table moves the fabrication chamber linearly under the laser beam. The advantage of this dedicated test bench over a commercial-like machine is to be able to look as closely as possible at the laser-matter interaction. This setup enables a continuous monitoring of the laser-melt-pool interaction. A series of experiments have been carried

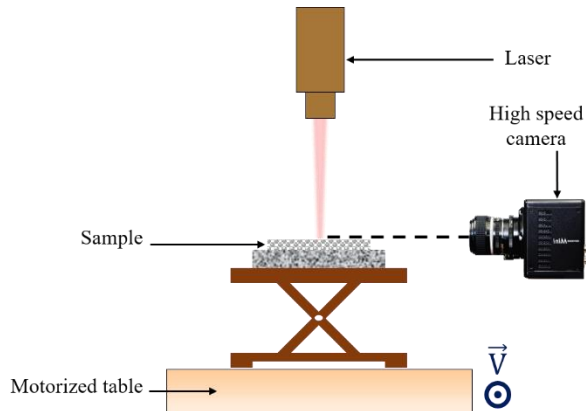


Figure 1 : Blueprint of the open L-PBF setup

out on single beads. The oxygen content in the chamber was intentionally varied from 2000 ppm to lower than 100 ppm, by varying the Argon flow through the diffuser. Intensity varied from 4 to 8  $\text{MW}\cdot\text{cm}^{-2}$ . The scan speed was constant at 500  $\text{mm}\cdot\text{s}^{-1}$ .

### Image analysis

An image analysis software was developed to study the tests records. Figure 2(a) presents the first step of this analysis: object detection. The system automatically recognizes spatters using blob detection method. The blob detection method relies on the stability of extremal regions through intensity ranges on the image. It enables to shape the outline of the particles. The intensity slightly varies between images because of the instable vapor plume. Yet, to simplify the system, the detection parameters remain strictly constant over time for the analyses. That is why, for some images with very intense plume, some error in particles detection might occur.

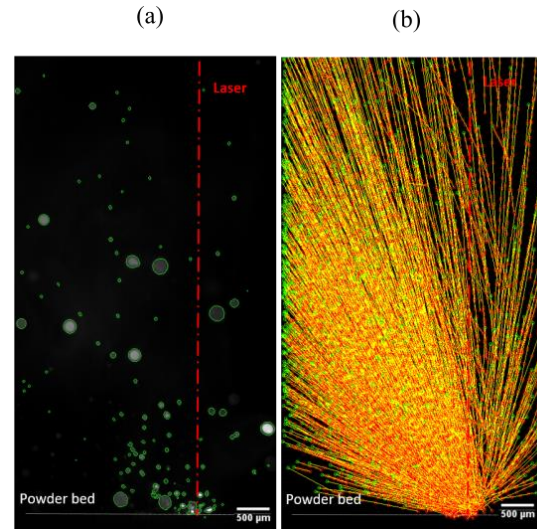


Figure 2 : (a) spatters detection; (b) spatters tracking during single bead melting in L-PBF

Moreover, it is difficult to detect both small and large spatters with the same accuracy, once again because extremal regions vary differently regarding the size of a particle. Therefore, compromises are necessary. In this case, authors optimized the detection parameters for the largest spatters, since they are the most harmful to the process. It means that small particles close to the feedstock powder size might not be detected by the system. However, the precision should be optimal regarding the large ones.

The precision and the sensitivity of the system are later evaluated through manual counting of spatter particles. A dataset is created by annotating a small subset of images. This dataset is then compared to the data resulting from the detection system. Four categories are distinguished, as described in Table 1.

*Table 1 : Confusion matrix used to evaluate the performance of the detection system by comparing the results with the actual dataset*

		Manual dataset	
		Spatter	No spatter
Detection system	Spatter	True Positive (TP)	False Positive (FP)
	No spatter	False Negative (FN)	True Negative (TN)

For example, a True Positive (TP) is a spatter correctly predicted by the system, while a False Negative (FN) is a spatter actually in the image but missed by the system. Precision and recall are then defined as follows:

$$P = \frac{TP}{TP + FP} \quad (1)$$

$$R = \frac{TP}{TP + FN} \quad (2)$$

In this study, precision is close to 100% while the recall is about 50%. These results were expected and ensue from the detection parameters as previously explained. This means that every particle identified by the system is indeed a spatter, but only half of the actual objects present in the videos are recognized as spatters. Manual counting demonstrated that most of the FN were particles included in the initial powder size distribution. As they are not supposed harmful to the process, it is estimated that their absence in the detection results is not detrimental for this analysis, and the statistic bias related to object detection is constant.

Figure 2(b) presents the second step of the analysis: tracking. The system automatically follows the particles from frame to frame, to determine the spatters trajectories, as well as their velocities and angle of ejection. In traditional methods previously mentioned, spatters analyses were performed on the cumulated detected particles. This led to a bias in the study as the fast particles are present in fewer images than the slow ones, inducing an over-estimation of the latter. In this work, only the particles that persisted over more than five frames are considered, which increases the accuracy of the collected data. *In fine*, this system gives

several information on the spatters generated during laser-matter interaction: number, size, speed, ejection angle to the laser beam.

## Materials

In this study, four aluminum alloys are compared:

- Two well-known casting alloys : AlSi<sub>7</sub> and AlSi<sub>10</sub>. These precipitation hardening alloys are close to eutectic point, leading to good castability and reducing hot cracking sensitivity.

- Two thermally stable aluminum alloys designed specifically for laser powder bed additive manufacturing: CTEC1 and CTEC2. These prototype solutions were developed by Constellium C-TEC. CTEC1 is an alloy from the Al-Fe-Zr system. CTEC2 is an Al-Mn-Cu-Ni-Zr alloy, as studied by Buttard *et al.* [13]. The alloys do not contain volatile elements such as Zn and Mg which tend to vaporize under the laser.

The four alloys powders have a spherical shape and their particle sizes are described in Table 2.

*Table 2 : Size distribution of the four aluminum alloys determined by laser diffraction*

Al alloys	R10 [μm]	R50 [μm]	R90 [μm]
AlSi <sub>7</sub>	17	22	28
AlSi <sub>10</sub>	17	21	25
CTEC1	15	19	25
CTEC2	14	20	26

The powder is spread on 3 mm thick metal substrate of same composition as the powder. Single beads are performed on 120 μm thick powder bed. This thickness is chosen to facilitate the implementation of the experiment, and to have a sufficient amplitude to observe the physical phenomena. Besides, in L-PBF machine the powder layer thickness gradually increases during the first layers, because of the powder density (usually about 50%) [14]. 120 μm is thus representative of the powder thickness after successive layers for a constant 60 μm plate displacement.

## Results

### Influence of oxygen content in the chamber

Spatters size distribution, speed, and orientation were examined for three different chamber atmospheres: O<sub>2</sub> content of 2000 ppm, 400 ppm and under 100 ppm. The standardized distribution were compared. Figure 3 presents the results for AlSi<sub>10</sub> detected spatters at 5.66 MW.cm<sup>-2</sup>. N is the number of detected particles per

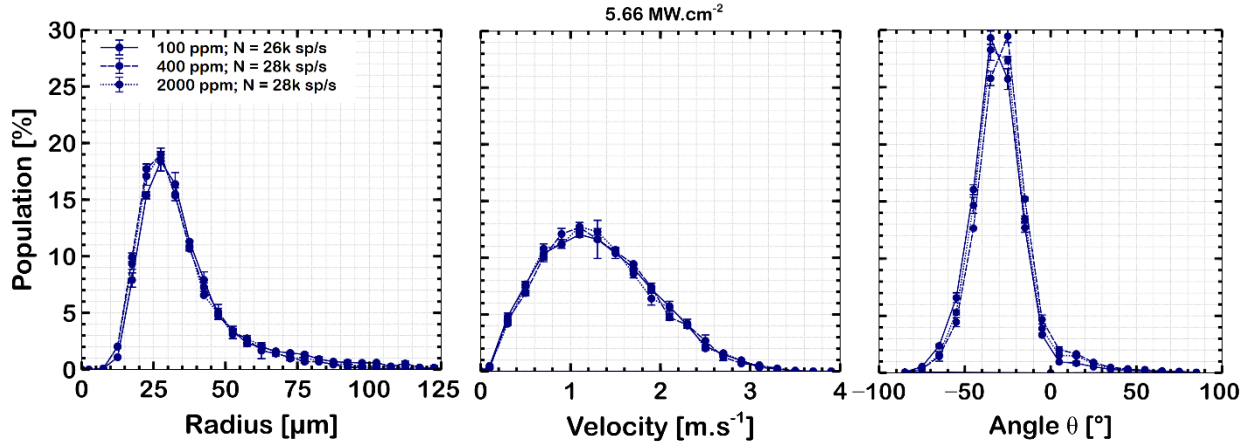


Figure 3 : Identical standardized size, velocity and angle distributions of  $\text{AlSi}_{10}$  spatters for different  $\text{O}_2$  content in the chamber at  $5.66 \text{ MW.cm}^{-2}$  (also observed at  $4.24 \text{ MW.cm}^{-2}$  and  $7.07 \text{ MW.cm}^{-2}$ )

second. The results show that a 20 times increase in the oxygen content does not affect the spatters distributions, as the curves mostly overlap. Same results are observed for all the intensities tested, for each of the four aluminum alloys. All the following results in this paper come out of trials under 100 ppm of  $\text{O}_2$  in the chamber.

#### Influence of laser intensity

Figure 4 presents the evolution of spatters mean velocity according to intensity for three identical trials on  $\text{AlSi}_{10}$ . Intensity was varied from 4 to 8  $\text{MW.cm}^{-2}$ . The mean velocity considers all the particles detected and tracked during one trial at one given intensity. Firstly, the results highlight the reproducibility of the trials. Secondly, it appears a linear increase of the mean velocity with intensity, by a  $15.10^{-6} \text{ cm}^3.\text{J}^{-1}$  factor.

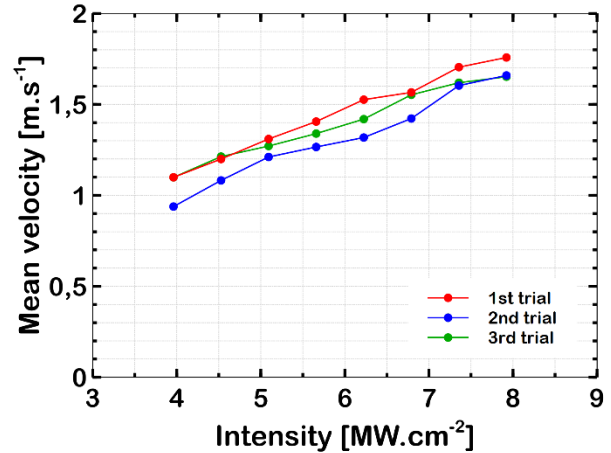


Figure 4 : Evolution of spatters mean velocity according to intensity, for three identical trials on  $\text{AlSi}_{10}$

Figure 5 presents the cumulated position of the detected spatters and illustrates the well-known evolution of the ejection angle  $\theta$  to the laser beam, for three different intensities for  $\text{AlSi}_{10}$ . The results show that  $\theta$  increases with intensity. This phenomenon is well known in laser welding [15] and has also been observed in L-PBF for high laser scan speed [1]. A wide  $\theta$  angle is responsible for a large spatter contaminated zone on the powder bed.

Figure 6 presents the standardized size distribution of detected spatters for  $\text{AlSi}_{10}$  for three different intensities, as well as the particle size distribution of the feedstock powder. The results show similar trends for all the intensities, with an asymmetric distribution and a peak at 20% of the total population for the dominant size category. A translation of the size distributions appears as the intensity increases. Besides, one can note a decrease in the number of detected particles per second for the highest intensity. One explanation could be the cumulated effect of the particle's speed and orientation.

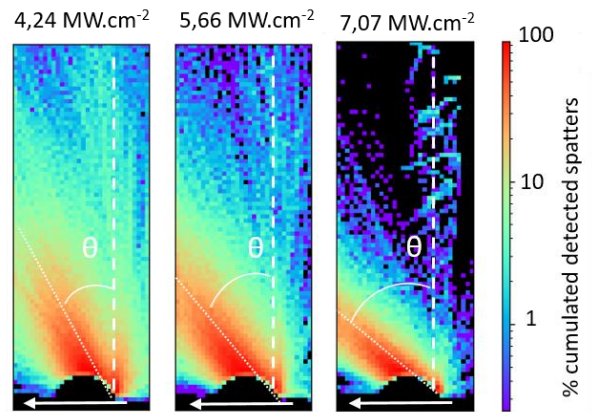


Figure 5 : Evolution of the ejection angle  $\theta$  to the laser beam, for three different intensities for  $\text{AlSi}_{10}$



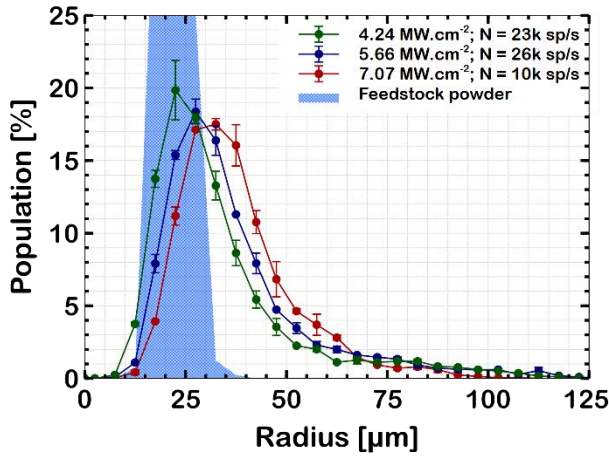


Figure 6 : Standardized size distribution of detected spatters for AlSi<sub>10</sub> for three different intensities

Indeed, with a greater horizontal component of the trajectory and a higher velocity, the particles tend to leave the camera's field of view hastily. They are less likely to be detected on several frames beyond a certain velocity, and thus to perform tracking. This speed limit depends on the particle's trajectory angle, not only  $\theta$  but also along the depth of field. This mostly seems to affect the small particles close to the powder size distribution, as the speed increase is inversely proportional to the size. However, it is considered once again that these missed spatters are not harmful to the process, so their absence is not detrimental to this analysis.

#### Analysis of contamination level

A spatter is defined as pollutant if its size is out of the feedstock powder size distribution. These pollutant spatters are usually ejected from the melt-pool, or form agglomerates of melted particles. These large spatters are the most harmful for the process: by polluting the powder bed, they could hinder the recoating of the subsequent powder layer and generate inclusions. On the contrary, small spatters with a size distribution close to the initial feedstock powder are not considered damaging for the process, as the laser should melt them at the following layer. They usually stem from the powder bed entrainment by the vapor plume [1].

Data from Figure 6 make it possible to isolate the pollutant spatters, by comparing the standardized size distribution of detected spatters with the particle size distribution of the initial powder. Figure 7 presents the size division among the total detected spatters for AlSi<sub>10</sub> by using three different intensities. On one hand, it appears for 4.24 MW.cm<sup>-2</sup> that more than 50% of the detected spatters have a radius smaller than 30 μm and

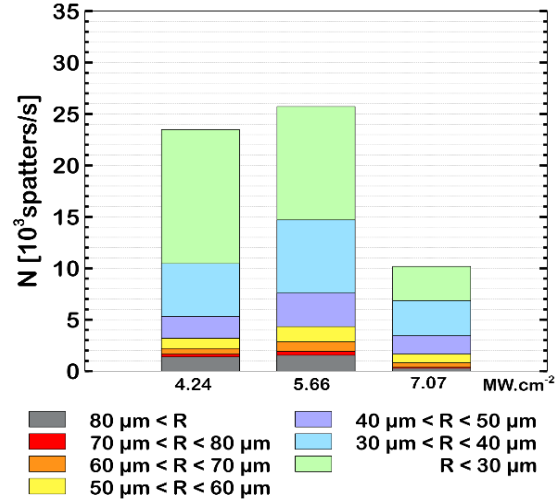


Figure 7 : Size division among the total detected spatters for AlSi<sub>10</sub> for three different intensities

thus may represent feedstock powder. This supports Ly's assessment that evaluates the vapor plume entrainment phenomenon as the dominant mechanism for spatter ejections, and therefore is responsible for the majority of the spatters detected [1]. In addition, it is alleged that part of the entrained feedstock powder is not detected for 7.07 MW.cm<sup>-2</sup> intensity, because of the significant velocity of the powder particles. On the other hand, particles with radius larger than 70 μm are emitted for every configurations represented here. Although these spatters represent a small percentage of the total spatters population, these particles can reach a volume thirty times bigger than the feedstock powder and be particularly prejudicial for the process.

#### AlSi comparison

Figure 8 presents two captures of the laser-matter interaction during a single bead fabrication at 5.66 MW.cm<sup>-2</sup>, comparing AlSi<sub>7</sub> with AlSi<sub>10</sub>. These pictures highlight the different behaviors of the two alloys. It visually seems that AlSi<sub>7</sub> generates more spatters than AlSi<sub>10</sub>.

Figure 9 presents the result of the analysis for AlSi<sub>7</sub> and AlSi<sub>10</sub> at 5.66 MW.cm<sup>-2</sup>. It shows the AlSi<sub>7</sub> emission rate is 30% higher than AlSi<sub>10</sub> one, which confirms the visual result previously mentioned.

#### AlSi vs AM alloys comparison

Figure 10 presents the analysis of the four aluminum alloys, for three different intensities. Figure 10(a) shows similarities between the different alloys, such as the 20% of total population peak for the dominant size category and the translation of the size distributions when intensity increases.

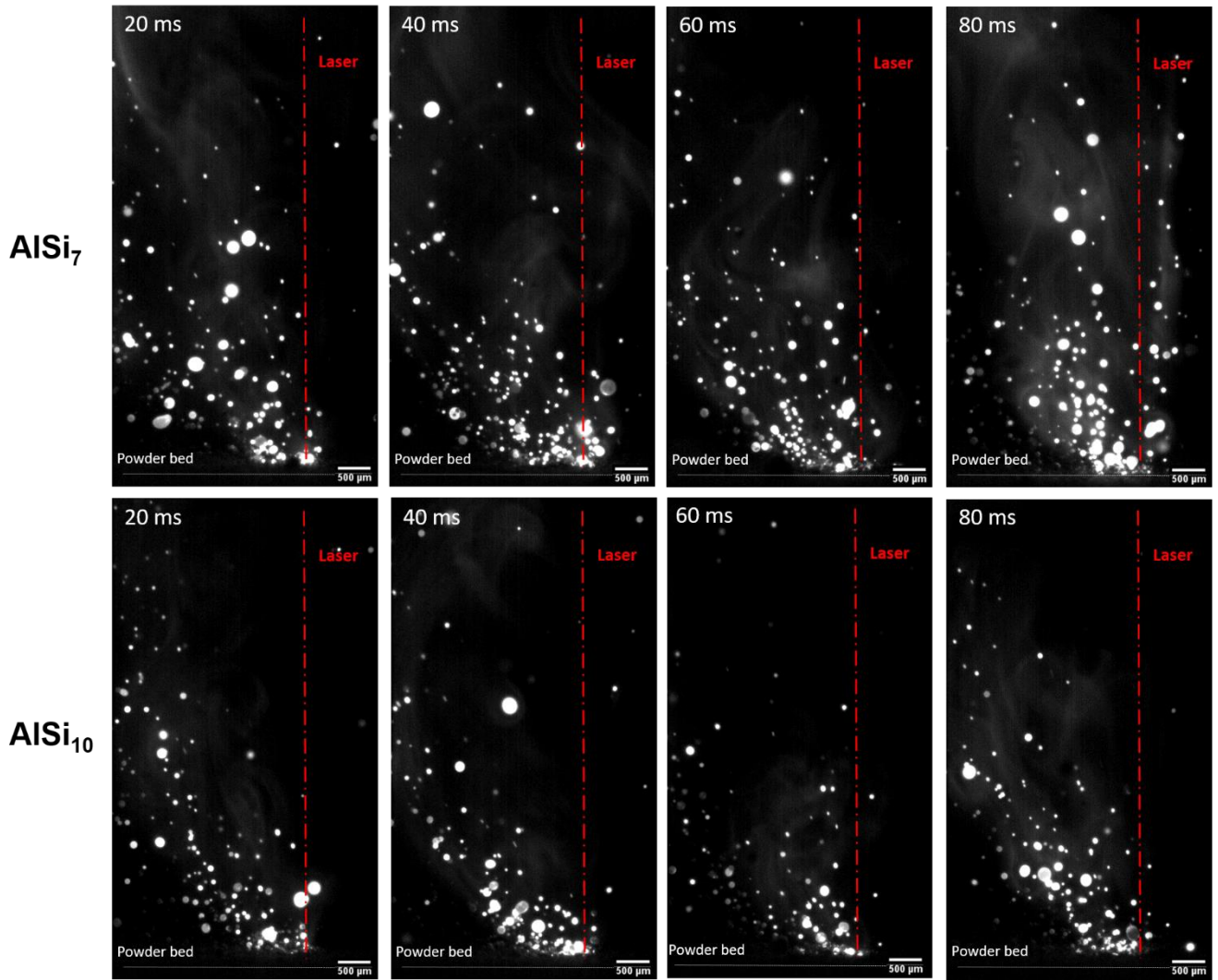


Figure 8 : Captures of the laser-matter interaction at different times during a single bead fabrication at  $5.66 \text{ MW.cm}^{-2}$ , comparing  $\text{AlSi}_7$  with  $\text{AlSi}_{10}$

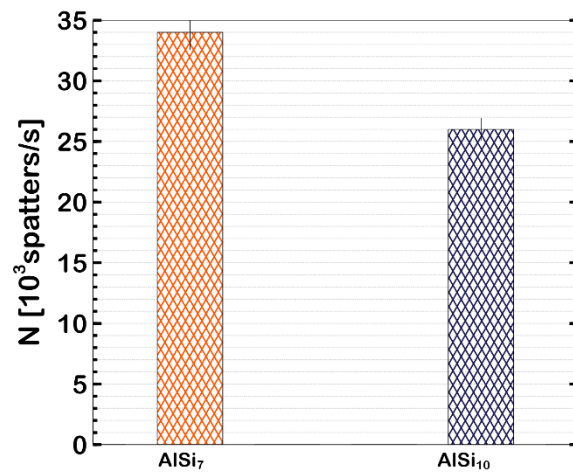


Figure 9 : Number of spatters per second for  $\text{AlSi}_7$  and  $\text{AlSi}_{10}$  at  $5.66 \text{ MW.cm}^{-2}$

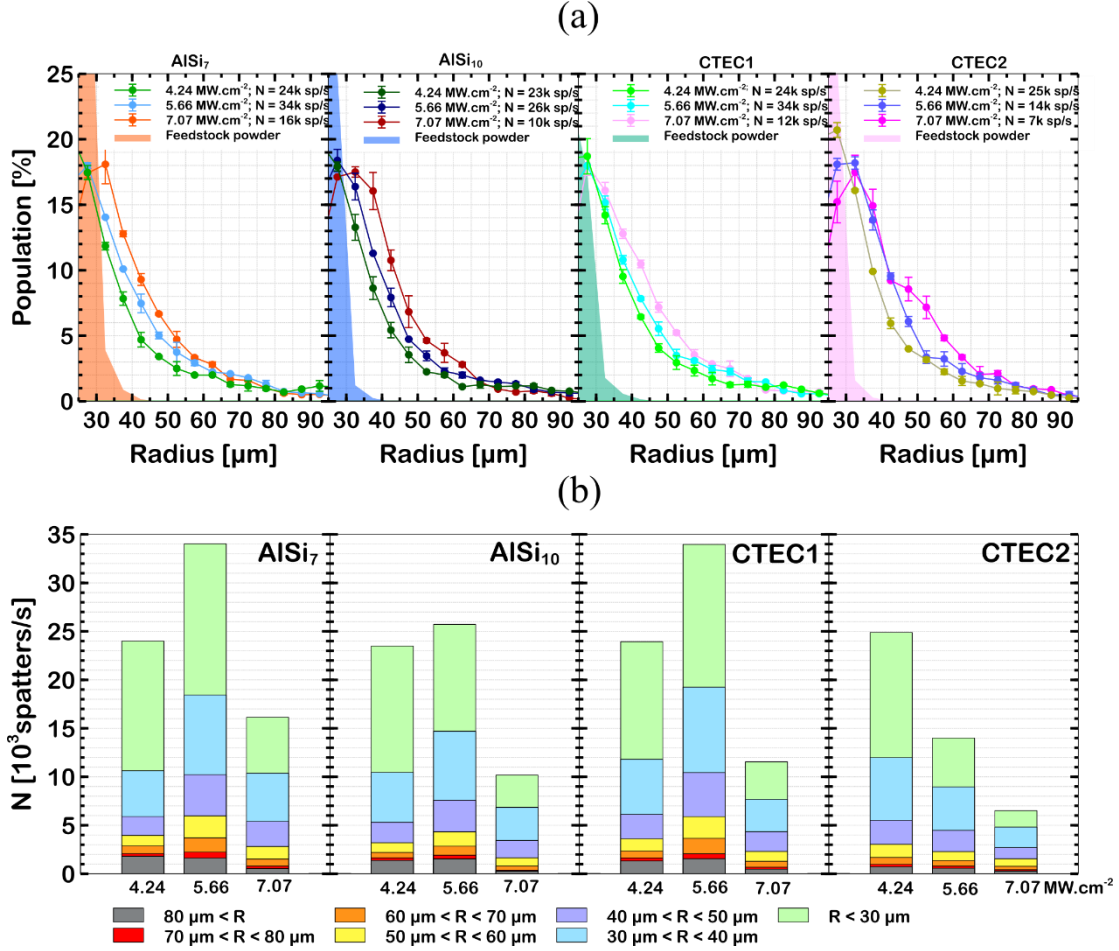


Figure 10 : (a) standardized size distribution of detected spatters (b) size division among the total detected spatters, for the four aluminum alloys, for three different intensities

By focusing on the largest particles ( $R > 80 \mu\text{m}$ ) in Figure 10(b), it is interesting to note that the lowest intensity seems to produce the highest number of spatter for the four alloys. This could result from a lowest gas pressure in the vapor plume at low intensity. By analogy with metal atomization, a higher gas flow separates the liquid into smaller droplets, as described by Thomas *et al.* [16]. Moreover, CTEC2 presents less spatters emission above  $80 \mu\text{m}$  than the AlSi alloys.

Figure 11 presents the spatters mean velocity for the four aluminum alloys as a function of intensity. Results show that CTEC2 spatters are 10 to 20% faster than the other alloys, especially at high intensity. This could be an explanation for the drop in detected spatters close to the feedstock powder size compared to other alloys as shown in Figure 10; they might be too fast to be detected.

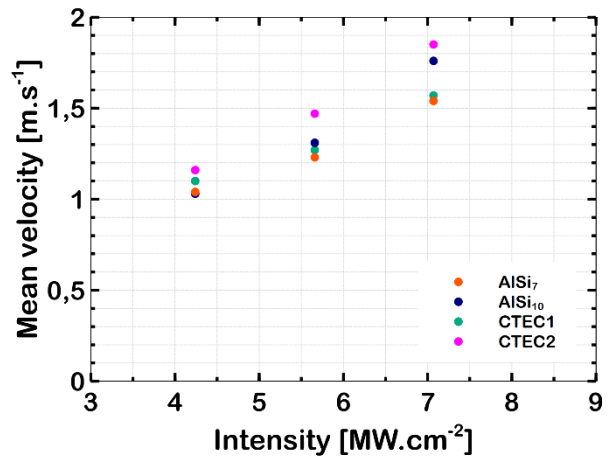


Figure 11 : Spatters mean velocity for the four aluminum alloys according intensity



Figure 12 presents the ejection angle  $\theta$  to the laser beam, for the four aluminum alloys at  $5.66 \text{ MW.cm}^{-2}$ . Results show that  $\theta$  is smaller for CTEC1 alloy, meaning that the spatters are ejected more vertically. On the opposite,  $\theta$  is larger for CTEC2, meaning the spatters are skimming the powder bed when ejected. This angle strongly influences the type of spatters resulting and their noxiousness.

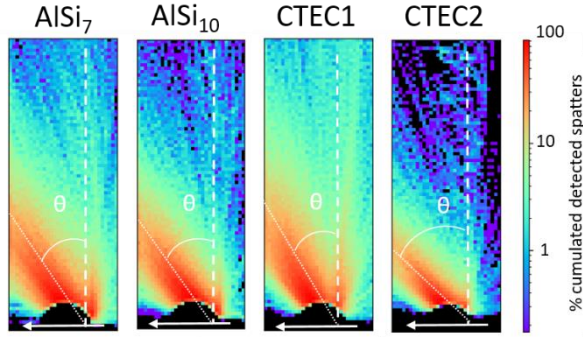


Figure 12 : Ejection angle  $\theta$  to the laser beam, for the four aluminum alloys at  $5.66 \text{ MW.cm}^{-2}$

## Discussion

### Image analysis

The image analysis software developed in this study presents only a 50% recall. It has been verified that the counted false negative were predominantly powder particles close to the feedstock size distribution. The misdetection of smaller particles could result from their high velocity. On the contrary, larger particles, which are slower, are accurately detected. As this study focuses on harmful spatters for L-PBF process, this low recall value do not impact the analysis. However, it would be interesting to improve the detection method to acquire more data. Current work is ongoing to detect spatters particles with machine learning algorithm. Moreover, it is essential to combine a great detection method to an effective camera set up. An additional camera would supplement the acquired information on the recorded videos.

### Oxygen impact on spatters

The influence of the oxygen content in the fabrication chamber has been addressed in this paper. It appears that a 20 factor variation of the  $\text{O}_2$  content does not affect the spatter ejection dynamic during L-PBF process. Oxygen has a strong impact on surface tension, especially for aluminum. This result demonstrates that surface tension does not have a significant impact on spatter ejection. It is known that the surface tension mostly affects the rear of the melt-pool with Marangoni effect [3], [17]. This effect on spatter ejection is proven

to be negligible compared to the vapor plume and the related recoil pressure effects. However, oxygen content can still have an impact on the spatters oxidation, which can decrease the mechanical properties of the final part. Hence, the minimum  $\text{O}_2$  content within the fabrication chamber is recommended.

### Influence of laser intensity

The results showed a linear increase in spatter mean velocity with the intensity. This phenomenon is directly related to the vaporization of the metal. The dragging force resulting from the vapor plume increases with the intensity and achieves hundreds of  $\text{m.s}^{-1}$ .

Moreover, results showed an increase of the ejection angle  $\theta$  to the laser beam with intensity, in accordance with laser welding [15]. The ejection angle strongly influences the impact of the spatter on the powder bed. For small  $\theta$  angle, the liquid droplet has enough time of flight to solidify and form a regular sphere. For great  $\theta$  angle, the droplet lands on the powder bed at liquid state and wet the surrounding powder particles to form an aggregate. In addition, in L-PBF machine, a spatter ejected vertically is more likely to be swept away by the cross-jet and be collected in the filter. If there were no such device, it will still fall near the laser beam and rapidly be melted. On the contrary, a spatter ejected far from the laser-matter interaction should pollute the powder bed and hinder the recoating of the next layer [4].

Besides, the effect of these spatters needs to be analyzed by considering the spatter size. Results showed an increase in spatter size as the intensity increased from  $4.24$  to  $7.07 \text{ MW.cm}^{-2}$ , for AlSi alloys as well as CTEC1. As previously mentioned, the dominant effect on spatter ejections is the recoil pressure, which intensifies with the laser intensity. This can explain the presence of more liquid metal jet expulsion and thus more pollutant spatters.

### Materials comparison

The results showed similar behavior of the four aluminum alloys for  $4.24 \text{ MW.cm}^{-2}$  intensity, before moving apart for higher intensity. Although CTEC2 seems to generate fewer spatters, its wide orientation angle  $\theta$  increases the probability for its spatters to be harmful for the process compared to the other alloys because they are spread on the powder bed. As for CTEC1, it seems to generate similar spatters than AlSi but its ejection angle  $\theta$  leads to more vertical spatters direction. Overall, CTEC1 spatters could be less detrimental for L-PBF process than the AlSi alloys ones. Mechanical property testing should be performed to confirm this.

Differences between AlSi<sub>7</sub> and AlSi<sub>10</sub> behavior could result from the silicon rate difference between the two alloys. The latter can affect the solidification interval as well as the viscosity and thus influence the melt-pool hydrodynamics. The thermo-physical properties of these four different alloys could indeed affect the spatter generation and explain their differences. A better thermal conductivity could lead to a deeper penetration and thus modify the ejection angle  $\theta$ . This hypothesis is to be verified by characterizing the materials properties. The quantity of low vaporization point elements within the alloys is also to be compared, as it should affect the vapor plume.

### Conclusion

State of the art revealed a need to understand factors that influence spatter formation in L-PBF. This can be performed thanks to *in-situ* control methods. The observation of the laser-matter interaction via an open L-PBF set up offers a good compromise between cost and ease of implementation. The automated analysis method developed in this study enables to acquire qualitative and quantitative data on spatter ejections. Although the recall is to be improved, the detected particles were found to provide a sufficiently representative sample to perform multi-parameters comparisons. These analyses highlight the following results:

- A 20 times variation of oxygen content inside the fabrication chamber induces less than 10% difference on the number of spatters ejected. It also induces less than 5% difference on the size of these spatters, their velocity or their ejection angle. The spatter generation dynamic is thus independent of the oxygen content; by extension, the effects of the surface tension are negligible regarding spatter ejections. However, the oxygen content can still affect the material properties regarding the oxide layer and need to be minimized in the chamber.

- The spatters velocity increases linearly with the intensity. In addition, the spatter ejections angle widens with intensity, leading to more agglomerates and larger polluted zones on the powder bed. Higher intensity is also more likely to produce larger spatters. All these results can be linked to the metal vapor plume and its associated recoil pressure.

- A pollution rate can be determined when comparing the spatter size distribution with the feedstock powder. It supports the hypothesis that the predominant mechanism in spatter ejections is vapor plume entrainment of the powder bed particles. However, the larger spatters are the most harmful to the process.

- Different aluminum alloys present different behavior at the laser-matter interaction. It appears that alloys dedicated to AM lead to fewer spatters or less harmful ones than AlSi alloys. This can result from their chemical composition as well as their thermo-physical properties. Further materials characterization is needed to confirm these hypotheses.

To conclude, this global method helps in understanding the laser-matter interaction and especially the spatter ejection during L-PBF process. The data returned by the system could be useful to optimize laser strategies in L-PBF in order to reduce defects caused by spatters. The assessment of powder bed's pollution rate is also a good indicator for powder reusing. The final objective will be to relate the process conditions with the spatters statistic distributions, to ensure AM process control.

### Acknowledgment

This work was supported by the Additive Factory Hub (AFH) in France.

### References

- [1] S. Ly, A. M. Rubenchik, S. A. Khairallah, G. Guss, and M. J. Matthews, "Metal vapor micro-jet controls material redistribution in laser powder bed fusion additive manufacturing," *Sci. Rep.*, vol. 7, no. 1, pp. 1–12, 2017, doi: 10.1038/s41598-017-04237-z.
- [2] V. Gunenthiram *et al.*, "Experimental analysis of spatter generation and melt-pool behavior during the powder bed laser beam melting process," *J. Mater. Process. Technol.*, vol. 251, pp. 376–386, 2018, doi: <https://doi.org/10.1016/j.jmatprotec.2017.08.012>.
- [3] D. Wang *et al.*, "Mechanisms and characteristics of spatter generation in SLM processing and its effect on the properties," *Mater. Des.*, vol. 117, pp. 121–130, 2017, doi: 10.1016/j.matdes.2016.12.060.
- [4] Y. Liu, Y. Yang, S. Mai, D. Wang, and C. Song, "Investigation into spatter behavior during selective laser melting of AISI 316L stainless steel powder," *Mater. Des.*, vol. 87, pp. 797–806, 2015, doi: 10.1016/j.matdes.2015.08.086.
- [5] M. Lutter-Günther, M. Bröker, T. Mayer, S. Lizak, C. Seidel, and G. Reinhart, "Spatter formation during laser beam melting of AlSi10Mg and effects on powder quality," in *Procedia CIRP*, 2018, vol. 74, pp. 33–38, doi:

- 10.1016/j.procir.2018.08.008.
- [6] D. You, X. Gao, and S. Katayama, "Visual-based spatter detection during high-power disk laser welding," *Opt. Lasers Eng.*, 2014, doi: 10.1016/j.optlaseng.2013.09.010.
- [7] G. Repossini, V. Laguzza, M. Grasso, and B. M. Colosimo, "On the use of spatter signature for in-situ monitoring of Laser Powder Bed Fusion," *Addit. Manuf.*, vol. 16, pp. 35–48, 2017, doi: 10.1016/j.addma.2017.05.004.
- [8] C. Barrett *et al.*, "Low cost, high speed stereovision for spatter tracking in laser powder bed fusion," in *Solid Freeform Fabrication 2018: Proceedings of the 29th Annual International Solid Freeform Fabrication Symposium - An Additive Manufacturing Conference, SFF 2018*, 2020, pp. 2122–2134.
- [9] M. Taheri, R. Dehghani, M. R. Karamooz-ravari, R. Mirzaeifar, and J. Ni, "Spatter formation in selective laser melting process using multi-laser technology," *Mater. Des.*, vol. 131, pp. 460–469, 2017, doi: 10.1016/j.matdes.2017.06.040.
- [10] S. Traore *et al.*, "Influence of gas atmosphere (Ar or He) on the laser powder bed fusion of a Ni-based alloy," *J. Mater. Process. Technol.*, vol. 288, 2021, doi: 10.1016/j.jmatprotec.2020.116851.
- [11] Q. Guo, C. Zhao, L. I. Escano, Z. Young, and L. Xiong, "Transient dynamics of powder spattering in laser powder bed fusion additive manufacturing process revealed by in-situ high-speed high-energy x-ray imaging Acta Materialia Transient dynamics of powder spattering in laser powder bed fusion additive manufact," *Acta Mater.*, vol. 151, no. August, pp. 169–180, 2018, doi: 10.1016/j.actamat.2018.03.036.
- [12] Z. A. Young *et al.*, "Types of spatter and their features and formation mechanisms in laser powder bed fusion additive manufacturing process," *Addit. Manuf.*, vol. 36, no. June, p. 101438, 2020, doi: 10.1016/j.addma.2020.101438.
- [13] M. Buttard *et al.*, "Multi-scale microstructural investigation of a new Al-Mn-Ni-Cu-Zr aluminium alloy processed by laser powder bed fusion," *Materialia*, vol. 18, no. July, p. 101160, 2021, doi: 10.1016/j.mtla.2021.101160.
- [14] D. Wang, Y. Yang, X. Su, and Y. Chen, "Study on energy input and its influences on single-track, multi-track, and multi-layer in SLM," *Int. J. Adv. Manuf. Technol.*, vol. 58, no. 9–12, pp. 1189–1199, 2012, doi: 10.1007/s00170-011-3443-y.
- [15] R. Fabbro, "Melt pool and keyhole behaviour analysis for deep penetration laser welding," *J. Phys. D. Appl. Phys.*, vol. 43, no. 44, 2010, doi: 10.1088/0022-3727/43/44/445501.
- [16] M. Thomas, T. De Terris, and S. Drawin, "Impact des caractéristiques des poudres sur les propriétés des matériaux métalliques élaborés par fabrication," *Trait. Matériaux*, vol. 447, pp. 22–31, 2017.
- [17] S. A. Khairallah, A. T. Anderson, A. M. Rubenchik, and W. E. King, "Laser powder-bed fusion additive manufacturing: Physics of complex melt flow and formation mechanisms of pores, spatter, and denudation zones," *Acta Mater.*, vol. 108, pp. 36–45, Apr. 2016, doi: 10.1016/j.actamat.2016.02.014.